Geophys. J. R astr. Soc. (1974) **38,** 587–608

The Galapagos Spreading Centre: Lithospheric Cooling and Hydrothermal Circulation*

David L. Williams,
R. P. Von Herzen, J. G. Sclater and R. N. Anderson

(Received 1974 March 15)†

Summary

The spatial pattern of cooling near a spreading ridge crest was investigated with a suite of 71 precisely-navigated heat-flow stations on the Galapagos spreading centre, East Pacific, near 86°W longitude. Stations are on crust less than 1·0 My old on which bathymetry and sediment distribution are well known. Values vary from near zero to greater than 30 HFU (10^{-6} cal cm^{-2} s^{-1}). The average over the entire region is significantly less than that predicted by theoretical conduction models of a cooling lithosphere. We observe a regular variation of the heat-flow pattern with a wavelength of 6 ± 1 km approximately normal to the ridge crest. Heat-flow maxima are characteristically located near faults and local topographic highs. The locations of fields of small sediment mounds, apparently hydrothermal vents, are also restricted to these faulted, elevated areas of high heat flow. Near-axis, bottom water temperature anomalies of several hundredths °C were detected. The low average, the low minima in the heat-flow pattern, and the water temperature anomalies suggest that hydrothermal circulation accounts for approximately 80 per cent of the geothermal heat released near the ridge crest. We conclude that the hydrothermal circulation pattern is controlled by one or more of the following physical properties of the system: highly developed cellular convection, discrete zones of high permeability, variation in the strength of heat sources near the base of the crust, or bottom topography. Our results imply that heat-flow studies near active oceanic ridges will be of most value if they are sufficiently detailed and well navigated to define the systematic small-scale variations that appear to be caused by hydrothermal circulation.

Introduction

In modern theories of sea-floor spreading, new oceanic lithosphere is created by the cooling of hot material as it moves away from the axis of a spreading centre. This process is one of the major mechanisms by which the Earth releases heat (McKenzie & Sclater 1969; Sleep 1969; Williams & Von Herzen 1974). Even before these new tectonic theories were established, ridges were recognized as regions of generally high but extremely variable heat flow (Von Herzen & Langseth 1966). Despite a tremendous increase in the number of heat-flow determinations, with few exceptions, this characterization of active ridge axis heat flow still holds (Langseth & Von Herzen 1971). With the evolution of the sea-floor spreading hypotheses came the

*Contribution No. 3302 of the Woods Hole Oceanographic Institution, and contribution of the Scripps Institution of Oceanography, new series.
†Received in original form 1974 January 14

Downloaded from https://academic.oup.com/gji/article/38/3/587/674012 by guest on 20 August 2022

development of several theoretical models of a conductively cooling lithosphere (Langseth, Le Pichon & Ewing 1966; McKenzie 1967; Sleep 1969; McKenzie & Sclater 1969; Sclater & Francheteau 1970; Parker & Oldenburg, 1973). With reasonable input parameters, they all predict heat-flow values near the ridge axes (within a few tens of kilometres) much higher than have generally been measured. Further, the models do not predict the scatter or general pattern of conductive heat flow that is normally observed at a spreading centre.

Heat-flow measurements on spreading ridges suffer from several limitations. First, with presently existing techniques, oceanic heat-flow measurements are possible only in sediments, whereas active spreading centres are ideally and actually characterized by little or no sediment cover. This fact limits measurements to sea floor at least old enough to have accumulated a sufficient thickness (a few metres) of sediments. Second, local environmental effects, which can disturb the near surface geothermal gradient (Langseth & Von Herzen 1971; Von Herzen & Uyeda 1963) tend to be more severe near mid-ocean ridges. Topographic variations are large and the sediment tends to accumulate unevenly, with greater thicknesses in the topographic lows. Finally, these techniques only measure the conductive component of the heat flux. There is a growing amount of evidence that the failure of conductive-cooling models to explain the observations is due to other heat transfer mechanisms, primarily hydrothermal convection in the crustal rocks (Elder 1965; Pálmason 1967; Erickson & Simmons 1969; Le Pichon & Langseth 1969; Sleep 1969; Deffeyes 1970; Talwani, Windisch & Langseth 1971; Langseth & Von Herzen 1971; Hyndman & Rankin 1972; Lister 1972; Anderson 1972; Sclater & Klitgord 1973).

Other indications of hydrothermal circulation near mid-ocean ridge crests, e.g. hydrothermally altered rocks (Aumento, Loncarevic & Ross 1971; Miyashiro, Shida & Ewing 1971; Nishimori & Anderson 1974, in press), deposits from hydrothermal emanations (Corliss 1971; Sayles & Bischoff 1973), and ophiolitic rocks (Spooner & Fyfe 1973) provide qualitative evidence that this mechanism may be an important mode of heat transfer. The disparity between measured conducted heat-flow values and the theoretical models might determine directly the quantitative significance of this circulation for the cooling of an ideal lithosphere. For this reason one of the major goals of our investigation was to determine as accurately as possible the magnitude and distribution of the conducted heat flux near an active spreading centre.

The Galapagos spreading centre and the adjacent regions of the eastern equatorial Pacific have been the subject of numerous geological and geophysical studies (Herron & Heirtzler 1967; Raff 1968; Grim 1970; Herron 1972; van Andel & Heath 1973; Sclater & Klitgord 1973). Our study included a small area immediately south of the spreading centre near 86°W longitude (Fig. 1), a region recently investigated in some detail by Sclater & Klitgord (1973). The results reported here are part of a subsequent and more detailed study obtained on legs 6 and 7 (June–August 1972) of Expedition South Tow from R/V Thomas Washington of the Scripps Institution of Oceanography. Detailed studies of bathymetry, magnetics, sediment distribution and near-bottom water temperature structure from both surface-ship and deeply towed instruments are described in Klitgord & Mudie (1974), and Detrick *et al.* (1974). In this paper we discuss results of heat-flow and near-bottom water temperature measurements, and their implications for the thermal structure and the cooling of the young lithosphere of this region.

The sea floor is spreading north and south of the E–W trending spreading centre located near 0°48′N. latitude, at a half rate of about 34.4 mm/yr (Klitgord & Mudie 1974). This sea-floor spreading system is particularly suitable for our study because (1) the spreading history is well known, (2) the bottom topography is extremely two-dimensional and relatively subdued (Fig. 2), and (3) the sedimentation rate is high due to proximity to the equatorial high productivity belt. The latter two factors allowed heat-flow measurements to within 5 km of the spreading axis (on crust as young as

Downloaded from https://academic.oup.com/gji/article/38/3/587/674012 by guest on 20 August 2022

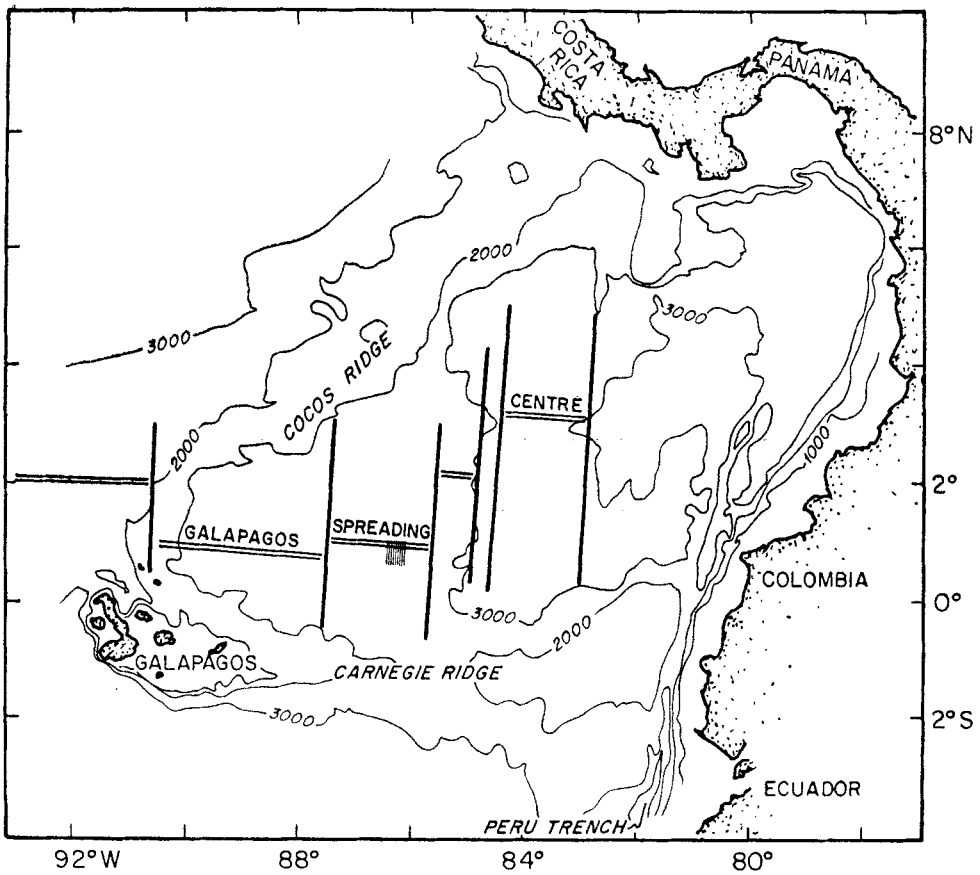

FIG. 1. Panama basin. Bathymetric contours are from van Andel *et al.* (1971) in uncorrected metres. Hatched lines mark area of detailed survey.

0·15 My), without significant bias in the location of each station due to the local sediment distribution.

Measurements and techniques

The 71 new heat-flow measurements (Table 1) and the bottom water temperature data reported in this paper were obtained on leg 7 of Expedition South Tow. Most of the temperature gradients in the sea floor were measured with probes designed for multiple penetrations of the sediments to depths up to 4m, with apparatus described previously by Von Herzen & Anderson (1972) and Corry, Dubois & Vacquier (1968). Two measurements of deeper penetration (greater than 10m) were made with thermistor probes attached to a piston corer. Thermal conductivity was determined by the needle probe method (Von Herzen & Maxwell 1959). The thermal conductivity of our piston cores averaged $1{\cdot}71 \times 10^{-3}$ cal cm^{-2} s^{-1} °C^{-1} for the upper two metres and $1{\cdot}80 \times 10^{-3}$ cal cm^{-2} s^{-1} °C^{-1} on the upper four metres. These values have been assumed, as appropriate, for the other stations (Table 1).

Navigation for both the leg 6 and leg 7 of Expedition South Tow surveys was accomplished utilizing, whenever possible, a net of 6 acoustic bottom transponders emplaced at the beginning of the leg 6 survey. On 12 of our heat-flow stations and both of the near-bottom horizontal water temperature profiles, the instrumentation was navigated inside the transponder net with near-bottom acoustic equipment attached to the hoisting cable (Boegeman *et al.* 1971); the positioning had an accuracy of $\pm$ 200 m relative to the bathymetry (Fig. 2). On an additional 10 heat-flow stations

Downloaded from https://academic.oup.com/gji/article/38/3/587/674012 by guest on 20 August 2022

Table 1.

Station No.	Lat. (°N)	Long. (°W)	Water depth	T	P	N	K	Q
43	0°50·3′	86°8·9′	2730		2·4	3	(1·71 (0·72))	0·25 (10) i
45(1)	0°50·9′	86°10·1′	2580		2·4	3	(1·71 (0·72))	4·42 (185) i
(2)	0°50·6′	86°9·9′	2630		0·7	1	(1·71 (0·72))	⩾ 2·22 (⩾92) i †
46	0°51·7′	86°8·8′	2620		2·4	3	(1·71 (0·72))	10·40 (436) v
50(1)	0°45·0′	86°7·4′	2690		2·4	3	(1·71 (0·72))	0·00 (0) v
(2)	0°44·8′	86°7·1′	2700	2·06	2·4	3	(1·71 (0·72))	1·30 (55) v
51	0°43·0′	86°6·7′	2600	2·05	2·4	3	(1·71 (0·72))	12·10 (507
52	0°44·5′	86°8·2′	2750	2·07	2·4	3	(1·71 (0·72))	2·41 (105) v
53(1)	0°45·7′	86°9·0′	2670	2·03	2·1	3	(1·71 (0·72))	⩾ 4.25 (⩾178) iw
(2)	0°44·9′	86°8·8′	2740	2·05	2·2	3	(1·71 (0·72))	⩾ 2·10 (⩾88) iw
54(1)	0°45·1′	86°7·8′	2690	2·04	2·5	3	(1·71 (0·72))	0·75 ± 0·03 (31 ± 1) w
(2)	0°44·9′	86°7·8′	2700	2·05	2·5	3	(1·71 (0·72)	1·07 ± 0·03 (45 ± 1) w
(3)	0°44·8′	86°7·8′	2680	2·04	2·9	3	(1·71 (0·72))	2·24 ± 0·15 (94 ± 6) w
(4)	0°44·5′	86°7·8′	2760	2·05	2·5	1	(1·71 (0·72))	⩾18·98 (⩾785) w
(5)	0°44·3′	86°7·9′	2760	2·05	2·9	3	(1·71 (0·72))	5·75 ± 0·47 (241 ± 20) w
(6)	0°43·8′	86°8·0′	2760	2·03	2·8	3	(1·71 (0·72))	6·18 ± 0·48 (259 ± 20) w
(7)	0°43·5′	86°8·0′	2590	2·03	2·5	2	(1·71 (0·72))	17·03 ± 1·00 (715 ± 22) w
(8)	0°43·1′	86°8·1′	2600	2·04	2·7	2	(1·71 (0·72))	⩾ 8·80 (⩾369) w
55(1)	0°42·2′	86°11·5′	2670		2·4	3	(1·71 (0·72))	1·90 (80)
(2)	0°42·0′	86°11·6′	2720		2·4	3	(1·71 (0·72))	3·24 (136)
(3)	0°41·7′	86°11·6′	2720	1·96	2·4	3	(1·71 (0·72))	1·03 (43)
56(1)	0°40·7′	86°11·5′	2770	2·06	2·4	3	(1·71 (0·72))	2·73 (104)
(2)	0°40·5′	86°11·5′	2730	2·06	2·4	3	(1·71 (0·72))	3·06 (128)
57(1)	0°36·6′	86°11·9′	2720		2·4	3	(1·71 (0·72))	3·35 (140) v
(2)	0°37·0′	86°12.1′	2720	2·06	2·4	3	(1·71 (0·72))	4·06 (170) v
58	0°44·3′	86°7·3′	2730	2·05	2·7	3	(1·71 (0·72))	2·15 ± 0·16 (90 ± 7) w
59(1)	0°41·7′	86°8·4′	2720	2·04	3·0	2	(1·71 (0·72))	1·19 ± 0·07 (50 ± 3) w
(2)	0°41·5′	86°8·3′	2720	2·04	2·8	2	(1·71 (0·72))	1·32 ± 0·07 (52 ± 3) w
(3)	0°41·2′	86°8·4′	2640	2·03	2·8	2	(1·71 (0·72))	⩾ 5·94 (⩾249) w
(4)	0°40·9′	86°8·7′	2680	2·04	3·0	2	(1·71 (0·72))	2·69 ± 0·11 (113 ± 5) w
(5)	0°40·6′	86°8·9′	2740	2·04	3·3	2	(1·71 (0·72))	⩾ 2·79 (⩾117) w
(6)	0°40·3′	86°9·2′	2690	2·04	3·0	2	(1·71 (0·72))	⩾ 2·12 (⩾89) w
60	0°38·3′	86°10·6′	2740	2·06	2·4	3	(1·71 (0·72))	9·20 (386)
61(1)	0°40·3′	86°10·2′	2740	2·06	2·4	3	(1·71 (0·72))	1·78 (75)
(2)	0°40·6′	86°9·9′	2750		2·4	3	(1·71 (0·72))	1·32 (55)
(3)	0°40·8′	86°9·6′	2730		2·4	3	(1·71 (0·72))	1·08 (45)
62	0°35·1′	86°11·1′	2720	2·04	*	2	1·73 (1·73)	4·63 ± 0·45 (194 ± 19) vw
63(1)	0°39·1′	86°12·0′	2740	2·04	2·5	3	(1·71 (0·72))	— 0·01 ± 0·03 (0 ± 1) vw
(2)	0°38·8′	86°12·0	2720	2·04	2·9	3	(1·71 (0·72))	5·62 ± 0·36 (236 ± 15) w

(3)	0°38·6′	86°11·9′	2720	2·04	3·0	3	(1·71 (0·72))	6·11 ± 0·36 (256 ± 15) iw
(4)	0°38·2′	86°11·9′	2650	2·04	2·9	3	(1·71 (0·72))	7·00 ± 0·22 (294 ± 9) w
(5)	0°37·9′	86°11·8′	2640	2·03	3·0	2	(1·71 (0·72))	11·88 ± 0·75 (497 ± 31) w
(6)	0°37·4′	86°11·7′	2660	2·04	2·9	3	(1·71 (0·72))	9·53 ± 0·52 (399 ± 22) w
(7)	0°37·0′	86°11·5′	2720	2·04	2·7	3	(1·71 (0·72))	5·31 ± 0·30 (223 ± 13) w
(8)	0°36·3′	86°11·3′	2720	2·04	2·6	3	(1·71 (0·72))	⩾ 2·00 (⩾84) w
(9)	0°36·4′	86°11·3′	2720	2·03	2·7	3	(1·71 (0·72))	1·87 ± ·06 (79 ± 1) w
(10)	0°36·0′	86°11·1′	2720	2·04	2·8	3	(1·71 (0·72))	⩾ 8·49 (⩾355) w
(11)	0°35·8′	86°11·0′	2720	2·03	2·8	3	(1·71 (0·72))	⩾ 7·72 (⩾324) w
64(1)	0°35·7′	86°10·9′	2720		2·4	3	(1·71 (0·72))	12·72 (533) v
(2)	0°35·6′	86°10·9′	2720		2·4	3	(1·71 (0·72))	19·00 (796) v
(3)	0°35·4′	86°10·9′	2720	2·05	2·4	3	(1·71 (0·72))	8·59 (360) v
65(1)	0°34·2′	86°10·6′	2720		2·4	3	(1·71 (0·72))	8·99 (376)
(2)	0°34·1′	86°10·5′	2720	2·05	2·4	3	(1·71 (0·72))	10·55 (442)
66(1)	0°33·1′	86°11·2′	2780	2·05	2·4	3	(1·71 (0·72))	2·31 (97) i
(2)	0°32·8′	86°11·1′	2780	2·05	2·4	3	(1.71 (0·72))	1·92 (80) i
67(1)	0°34·5′	86°8·7′	2720	2·04	2·7	2	(1·71 (0·72))	13·01 ± 0·68 (546 ± 29) w
(2)	0°34·1′	86°8·7′	2720	2·04	2·9	2	(1·71 (0·72))	10·12 ± 0·09 (421 ± 46) w
(3)	0°33·7′	86°8·8′	2700	2·03	2·9	3	(1·71 (0·72))	7·10 ± 0·44 (298 ± 46) w
(4)	0°33·4′	86°8·8′	2730	2·04	2·8	3	(1·71 (0·72))	5·24 ± 0·36 (215 ± 15) iw
(5)	0°33·0′	86°8·9′	2760	2·04	2·8	3	(1·71 (0·72))	3·62 ± 0·22 (152 ± 9) iw
(6)	0°32·8′	86°9·0′	2780	2·04	2·7	3	(1·71 (0·72))	4·36 ± 0·26 (183 ± 11) iw
(7)	0°32·4′	86°9·0′	2780	2·04	2·8	3	(1·71 (0·72))	8·43 ± 0·46 (353 ± 19) iw
68	0°34·0′	86°13·8′	2720	2·03	11·2	5	1·78 (0·75)	6·91 ± 0·31 (290 ± 13) w
69(1)	0°32·0′	86°10·7′	7770	2·03	2·9	3	(1·71 (0·72))	6·29 ± 0·17 (264 ± 7) w
(2)	0°31·8′	86°10·7′	2750	2·03	2·9	3	(1·71 (0·72))	7·66 ± 0·22 (322 ± 9) w
(3)	0°31·6′	86°10·7′	2750	2·03	2·9	3	(1·71 (0·72))	⩾ 9·31 (⩾390) w
(4)	0°31·1′	86°10·7′	2730	2·03	2·1	2	(1·71 (0·72))	⩾30·28 (⩾1270) w
(5)	0°30·8′	86°10·7′	2750	2·04	2·9	3	(1·71 (0·72))	8·49 ± 0·46 (356 ± 19) w
(6)	0°30·5′	86°10·6′	2790	2·04	2·9	3	(1·71 (0·72))	8·04 ± 0·44 (337 ± 18) w
(7)	0°30·2′	86°10·5′	2760	2·04	2·8	3	(1·71 (0·72))	⩾ 7·99 (⩾334) w
(8)	0°29·9′	86°10·4′	2780	2·04	2·9	3	(1·71 (0·72))	7·57 ± 0·22 (318 ± 9) w

T is bottom water temperature (°C).
P is the estimated sediment penetration (m) of lowermost probe used for temperature gradient measurements.
N is number of thermistors used for sediment temperature gradient measurements.
K is the thermal conductivity in 10^{-3} cal $°C^{-1}$ cm^{-1} s^{-1} (W m^{-1} $°K^{-1}$). Outer parentheses indicate values assumed from measurements on nearby piston cores.
Q is heat flow in 10^{-6} cal cm^{-2} s^{-1} (10^{-3} W m^{-2}). Measurements made by Woods Hole Oceanographic Institution are indicated by a w with values and probable errors of these computed according to methods as in Von Herzen & Anderson (1972). An additonal uncertainty of ± 10 per cent in the heat flow values results when the thermal conductivity is assumed. Unless otherwise annotated, minimum values result from a tilt greater than our instruments can measure (> 30 degrees off vertical). i, v represent measurements in which the instrument or vessel respectively were acoustically navigated.
*Station 62 - some penetration beyond 10 m was indicated. The difficulty of fixing the actual penetration depth is discussed in the text.
† Only one thermistor on scale.
§ Water depth in corrected metres.

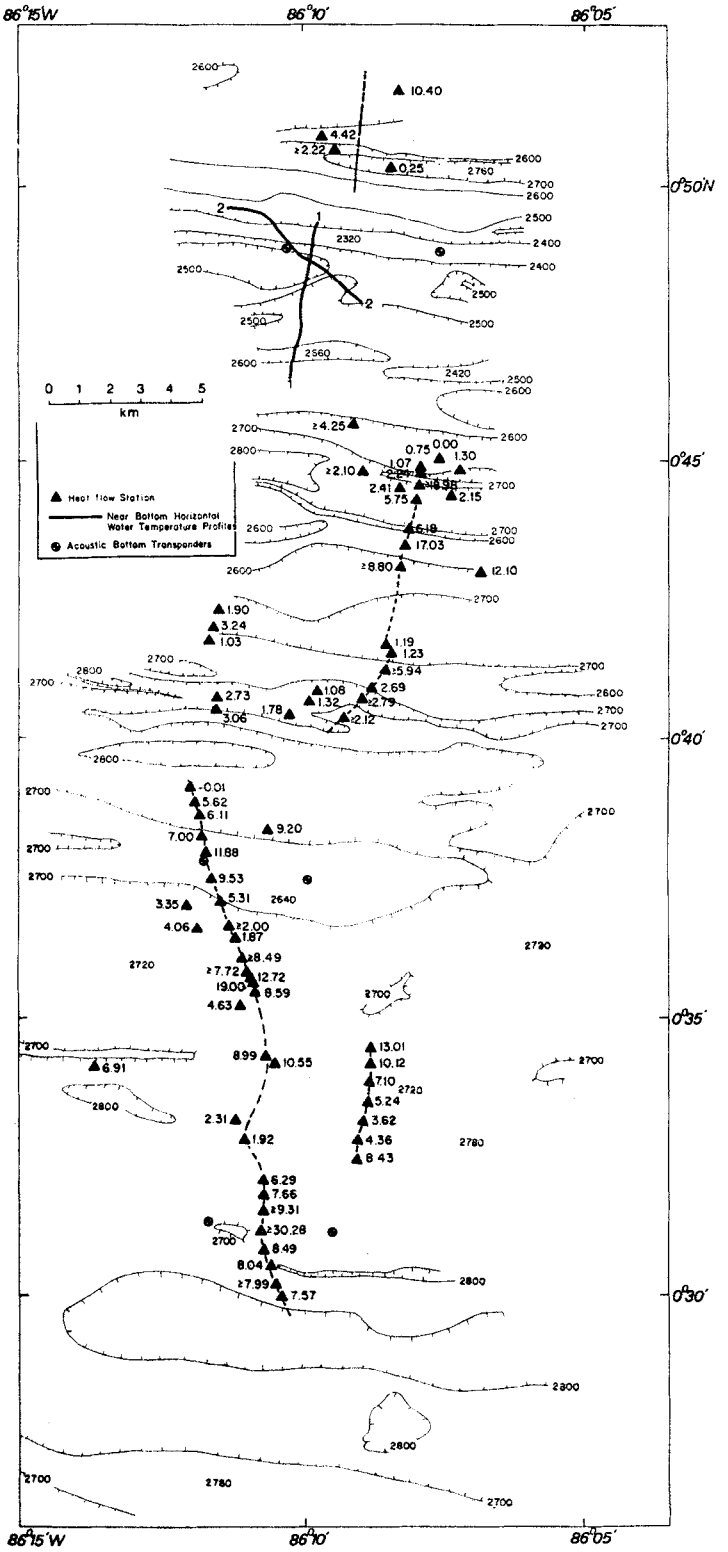

FIG. 2. Bathymetry and heat flow (HFU) in survey area. Dashed lines indicate location of topographic and heat-flow profiles illustrated in Fig. 8. Depths are in corrected metres at a 100 m contour interval.

Downloaded from https://academic.oup.com/gji/article/38/3/587/674012 by guest on 20 August 2022

it was possible to navigate the ship only acoustically. The position of the heat-flow measurement was determined from an empirical relation between wire angle and horizontal distance to the relay transponder on stations where relay transponder navigation was available. We estimate the uncertainty of station positions determined by this method at $\pm$ 400 m. No accoustic navigation was available for the remaining 48 heat-flow stations. These stations were located by a combination of satellite navigation, bathymetry (Klitgord & Mudie 1974), ranges to a single bottom transponder, and computer-generated dead reckoning. The quality of these positions varies appreciably but the average is probably no better than $\pm$ 1 km. Our ability to locate all our stations is somewhat better in latitude than longitude due to the east–west grain of the bottom topography. On most stations multiple penetrations were made. The relative positions between individual measurements on these stations are generally determined better than $\pm$ 300 m.

As many as 11 heat-flow measurements over horizontal distance of greater than 7 km were made during a single station with the multipenetration probe described in Von Herzen & Anderson (1972).

In addition to our heat-flow measurements, two near-bottom horizontal water temperature profiles were obtained utilizing the apparatus depicted in Fig. 3. The lower thermistor was generally maintained within 10 m of the sea floor. The temperature of each of the lower two thermistors was recorded twice every 30 s at different sensitivities. The upper thermistor temperature was recorded at high sensitivity once

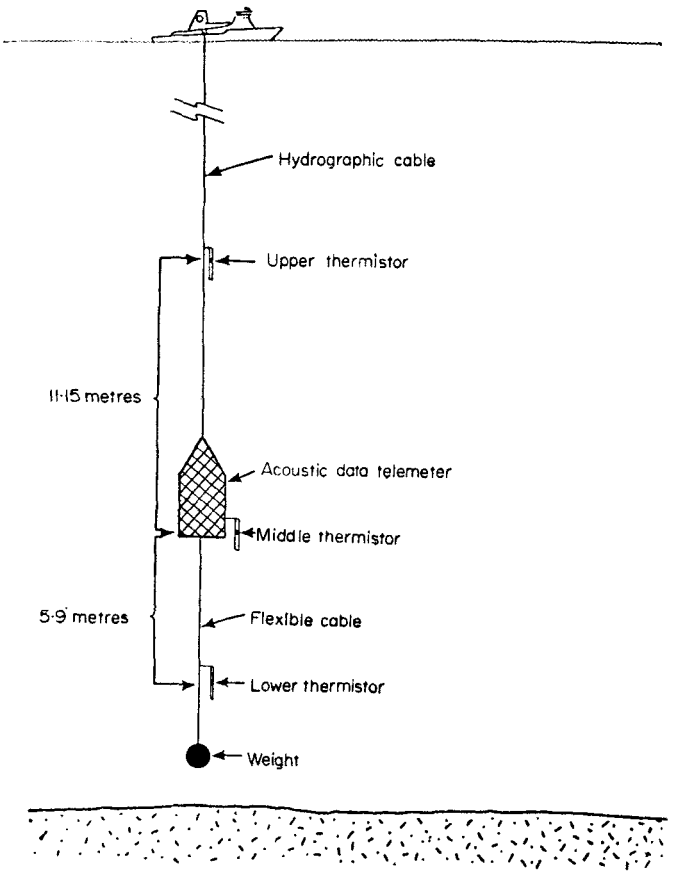

FIG. 3. Apparatus used in measuring horizontal water temperature profiles. Altitude above the bottom was maintained by echo sounding from the telemeter.

Downloaded from https://academic.oup.com/gji/article/38/3/587/674012 by guest on 20 August 2022

every 30 s. The potential temperatures have a precision of about ± 0·003°C at high sensitivity and ± 0·015°C at low sensitivity. Only the high sensitivity records are plotted in Fig. 8.

Observations

A synthesis of the heat-flow and water temperature data (Figs 2, 5, 6, 7, and 8) lead to the following observations: (1) conductive heat-flow measurements vary regularly from relatively low values averaging about 2×10^{-6} cal cm^{2-} s^{-1} (HFU) to high values averaging about 12 HFU, with extremes of individual measurements ranging from zero to greater than 30 HFU. A significant north–south variation in heat flow exists with a modulation wavelength of approximately 6 ± 1 km. (Fig. 5). It is clear from a close examination of Fig. 5, and particularly from the individual profiles in Fig. 6, that the heat-flow pattern is complicated. However, heat-flow maxima are marked by an absence of low values, and the heat-flow minima are almost as well defined. (2) The average heat flow gradually increases with distance south of the ridge

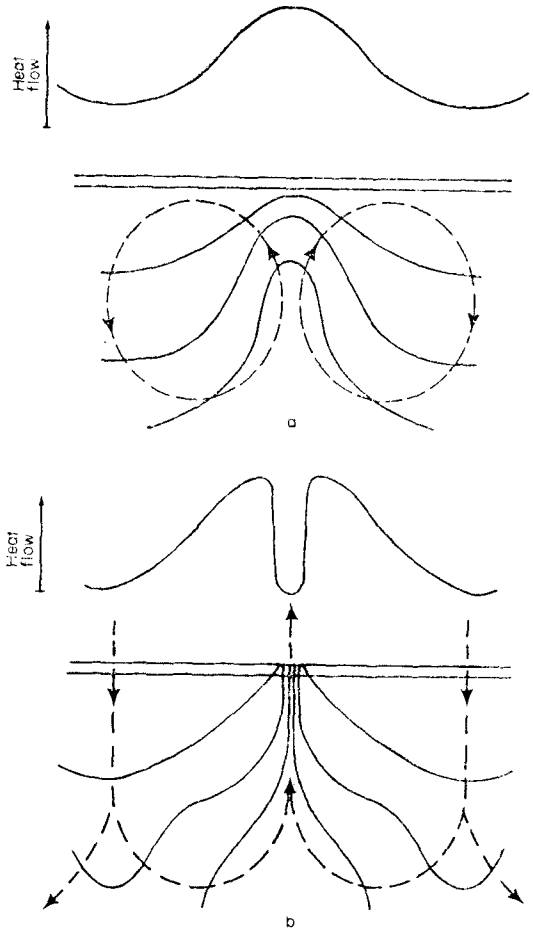

FIG. 4. Sketches illustrating the effect of hydrothermal circulation on geothermal gradients measured at the sea floor. Heavy solid lines represent isotherms, and dashed lines with arrows show the general pattern of convection. (a) Convection in crustal rocks below an impermeable sediment blanket. (b) Convection which penetrates the sediment cover allowing for exchange with the bottom waters. The effect on the conductive heat-flow pattern is shown above each sketch.

Downloaded from https://academic.oup.com/gji/article/38/3/587/674012 by guest on 20 August 2022

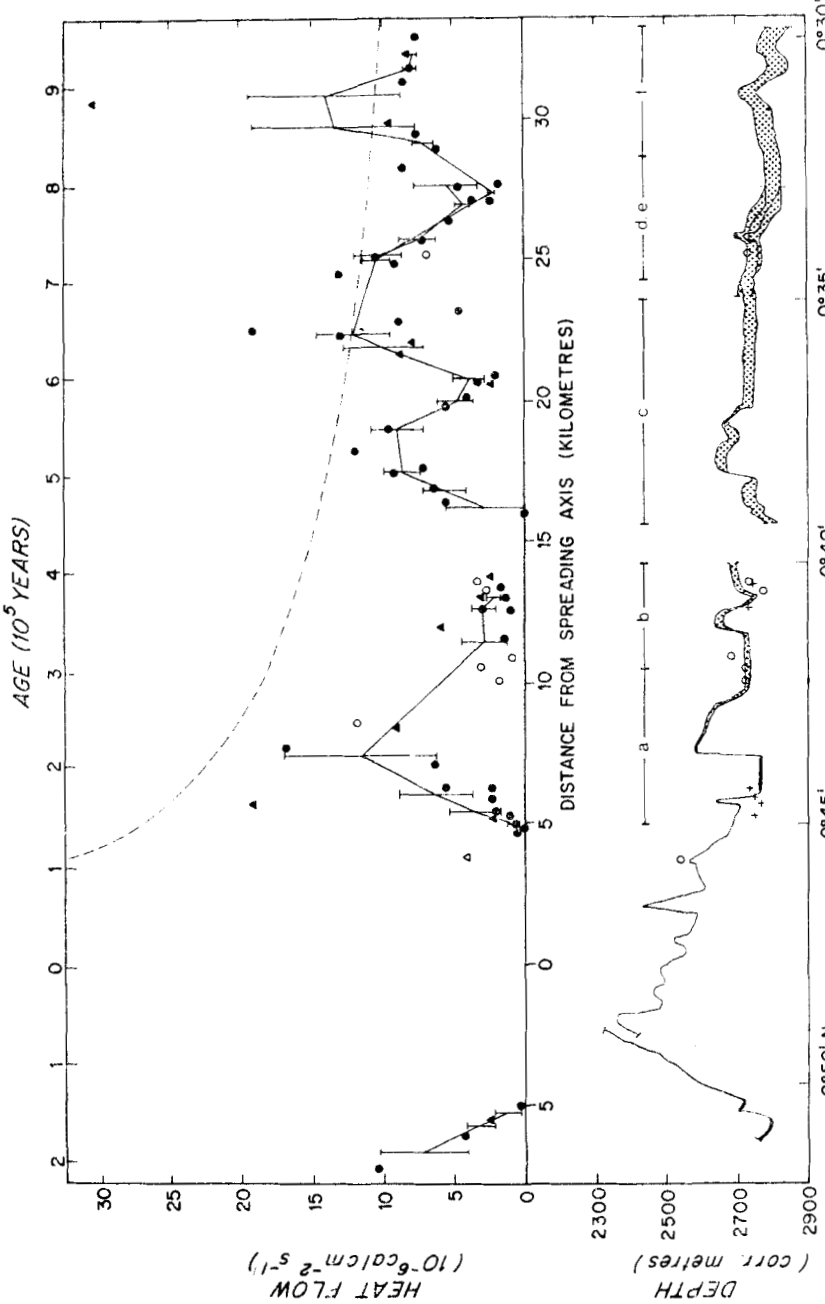

FIG. 5. Heat-flow data, topography and sediment thickness (stippled pattern) from the 4 profiles shown by dashed lines in Fig. 2 (projected north–south). The vertical exaggeration is 12·5:1. Closed circles are individual heat-flow values which were within 2 km of profile. Crosses represent depth of heat-flow measurement deviating 20 m or more from the plotted topography. Triangles indicate minimim values of heat flow. Open circles and triangles represent heat-flow stations more than 2 km away from the profile track. The circle with a cross in it is station 62. It is discussed in the text and is not used in the averages. The dashed line is the theoretical heat flow (from Sclater & Francheteau 1970) for an 85 km thick lithosphere, 1250°C on its lower boundary, an internal heat generation of $2{\cdot}0 \times 10^{-14}$ cal cm^{-3} s^{-1} and an average thermal conductivity of $6{\cdot}9 \times 10^{-3}$ cal cm^{-1} s^{-1}°C^{-1}. The solid lines connect averages of the measured heat flow values (vertical bars are ± standard error) averaged over 2 km intervals every 1 km along a profile.

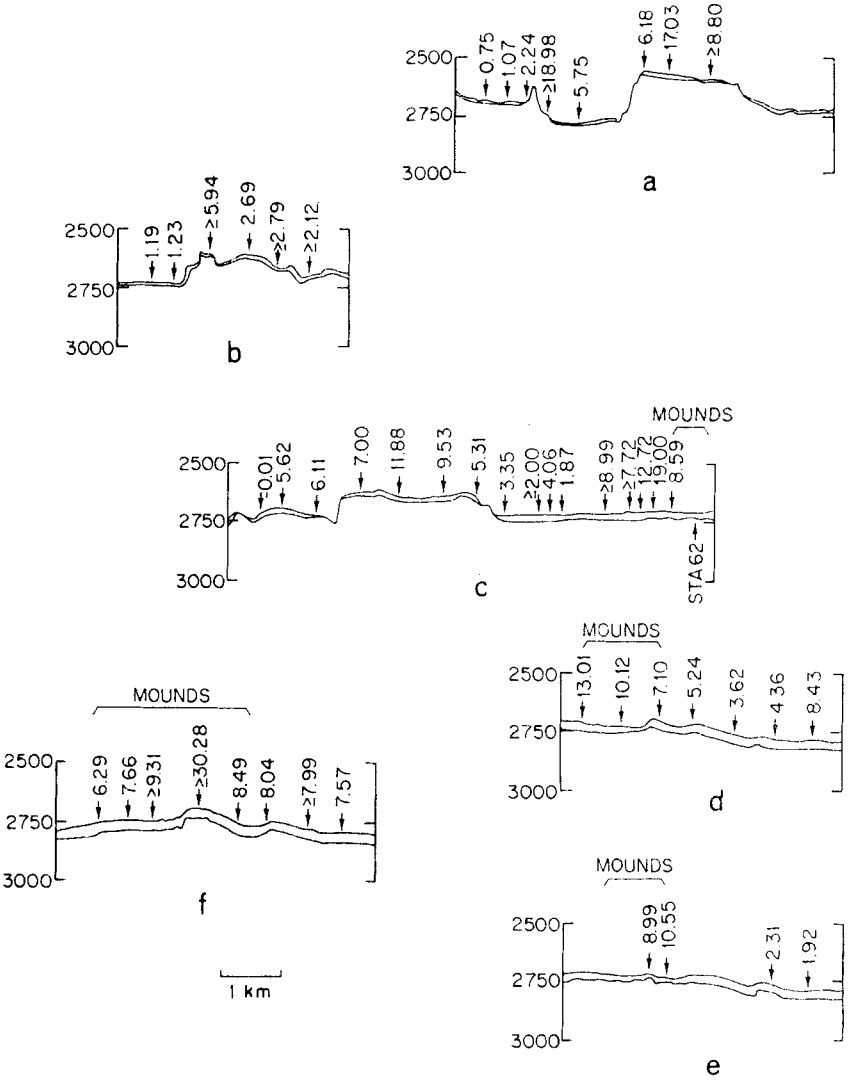

FIG. 6. Sediment and basement bathymetry from Klitgord & Mudie (1974). Each bathymetric profile is from an SIO deep-tow instrument package survey line that passes near the heat-flow station. The position of each profile is shown in Fig. 5. The location of mounds refers to the fields of sediment mounds discussed in the text. In general these mounds are too small to be seen at the vertical scale used in the figure. Numbers above the arrows are heat-flow values in 10^{-6} cal cm^{-2} s^{-1}. Depths are in corrected metres with a vertical exaggeration of 4:1. Since the heat flow stations were not located exactly on the bathymetric survey lines the relative geographical positions of the heat-flow stations have been adjusted to best reflect the actual bathymetry at the site of the heat-flow station. Only heat-flow measurements near each bathymetric profile are shown. As a result not all our measurements are illustrated.

Downloaded from https://academic.oup.com/gji/article/38/3/587/674012 by guest on 20 August 2022

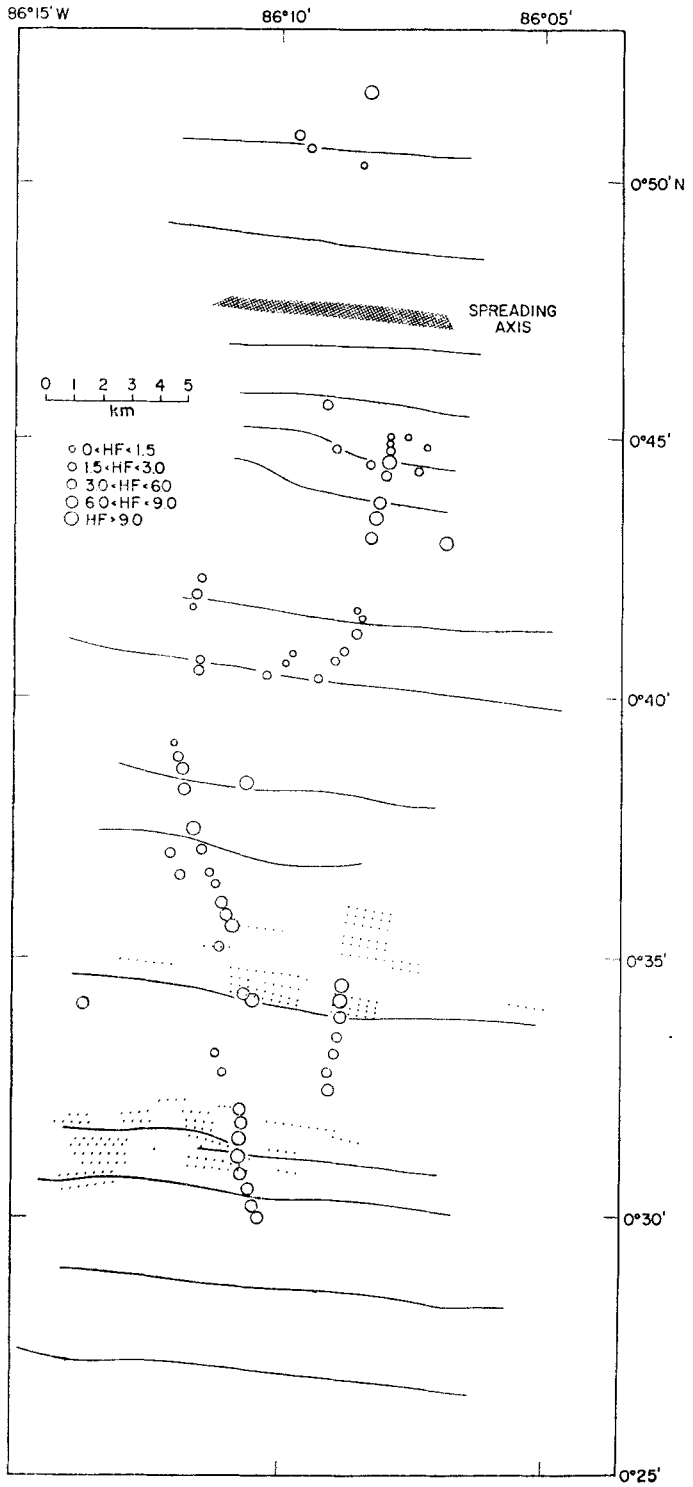

FIG. 7. A sketch map of our survey area. The heavy east–west trending dark lines mark the positions of fault scarps indentified by Klitgord & Mudie (1974). If these faults are zones of high permeability they could be important in the hydrothermal system. The small dots represent the general location of sediment mounds. Note the correlation of these mounds with areas of high heat flow.

Downloaded from https://academic.oup.com/gji/article/38/3/587/674012 by guest on 20 August 2022

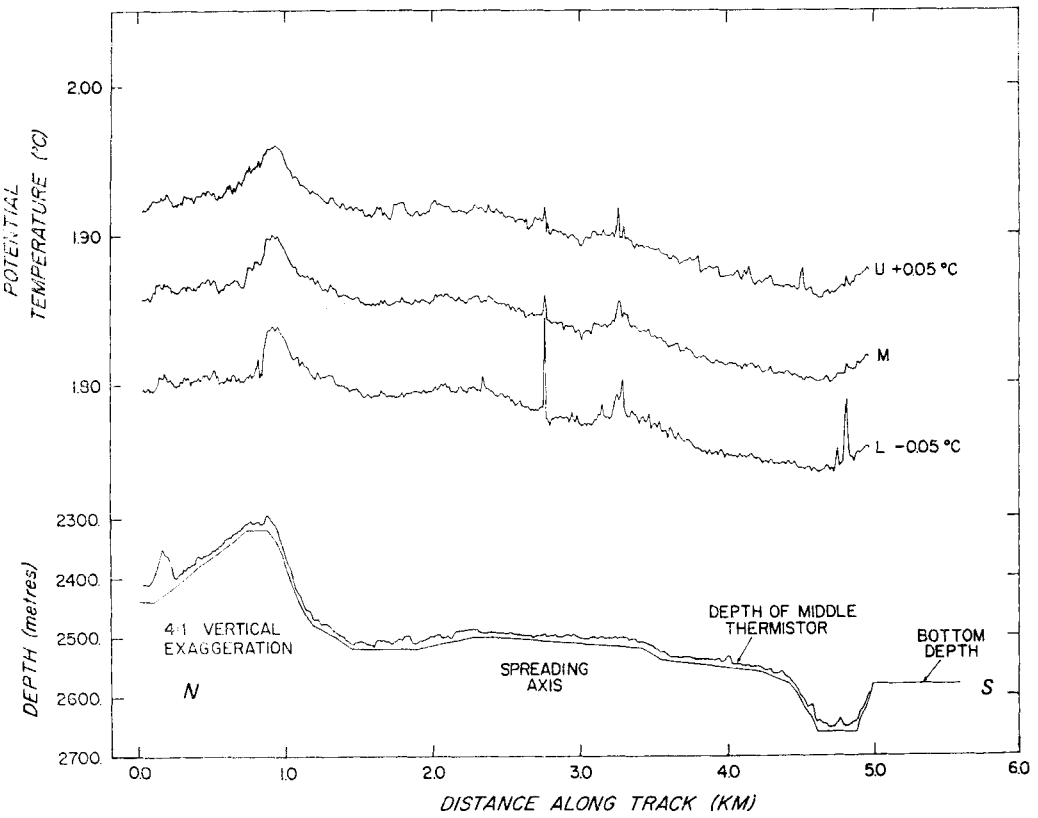

FIG. 8. Bottom water horizontal temperature profile, No. 1 (Fig. 2). U + 0·05°C is the potential temperature of the upper thermistor plus 0·05°C. M is the potential temperature of the middle thermistor and L −0·05°C is the lower thermistor potential temperature minus 0·05°C. The average horizontal speed was 1·28 km hr^{-1}. The thermistor depth trace shows much more roughness than the bottom because it is derived by subtracting a detailed thermistor altitude signal from less detailed bottom depth data. Therefore, much of the roughness in the thermistor depth is actually roughness of the bottom.

axis, whereas the theoretical heat flow, based on conductive cooling models (McKenzie 1967; Sclater & Francheteau 1970), decreases rapidly with distance from the axis (Fig. 5). (3) Near the spreading centre the average of the measured values is much less than the theoretical value but at the southern end of our survey this average clearly approaches the theoretical curve (Fig. 5). (4) The heat-flow minima tend to be on or near topographic lows and the heat-flow maxima are associated with either scarps, topographic highs, or fields of sediment mounds (Fig 5, 6 and 7). The mounds are found only in the southern half of our area an average about 5–10m high with a 25m radius, as determined from deep tow echo sounding and side-looking sonar (Klitgord & Mudie 1974). (5) On station 62 (Fig. 9) the observed thermal gradient extrapolated to the bottom water temperature yields an apparent penetration of 18·3 m for our 10 m piston core. Although there were other indications of some superpenetration, 8·3 m seems unlikely. (6) The average of all our measured heat-flow values is greater than 5·9 HFU. This is in good agreement with Sclater & Klitgord (1973). It is much higher than the world-wide average of conductive heat flow (1·5 HFU, Lee 1970). It is also significantly higher than has been measured at other spreading centres on crust of similar age (Langseth & Von Herzen 1971). (7) Several significant bottom water temperature anomalies can be seen in Fig. 8. The largest temperature anomaly is observed

Downloaded from https://academic.oup.com/gji/article/38/3/587/674012 by guest on 20 August 2022

over the regional topographic high, an east–west ridge located at 0°49′N latitude. This ridge apparently represents a boundary between different water types above and below the ridge crest, as observed by Sclater & Klitgord (1973) and Detrick *et al.* (1974). The other water temperature anomalies cannot be explained by bottom temperature structure or currents. Anomalies located at 2·76, 3·26 and 4·80 km along our track are significantly above the noise level of our measurements and appear on more than one sensor.

Interpretation

Conductive heat-flow measurements in a hydrothermal area

(a) *General.* Since we will use hydrothermal circulation to explain our observations it is worthwhile to discuss what we should expect from conductive heat-flow measurements in a hydrothermal area. Thermal gradients can be radically distorted by hydrothermal circulation. The sketches in Fig. 4 illustrate the effect of a hypothesized water circulation pattern on sub-surface isotherms. When the circulating system is confined to permable rock which is overlain by an impermeable sediment cap (Fig. 4(a)), larger thermal gradients will be measured above the rising limbs than above descending limbs. Thermal gradients should grade evenly between the limbs. But if the circulating system has free discharge and re-charge (Fig. 4(b)) thermal gradients near the axis of both rising and descending limbs can be quite small. In this case, since the sediment temperatures near the rising limb are much higher, it is still possible to separate these two causes. The pattern of heat flow between the limbs depends on the character of the system but we should find a heat-flow maximum adjacent to the discharge vent. More generally, the net effect of hydrothermal waters venting through the sea floor is to lower the regional geothermal gradient.

(b) *Heat-flow minima.* Since the Galapagos spreading centre appears to be actively spreading and thus is a volcanically active region, high temperature rock and magma can be expected near the surface. If conduction is the dominant heat transfer mechanism, we should find a consistently high geothermal gradient; instead we find regularly spaced minima. Occasional low gradients might be produced by sediment slumping (Von Herzen & Uyeda 1963) but the sediment distribution on the spreading centre is fairly uniform. Most steep basement slopes (fault scarps) tend to have thinner sediment cover, as expected; the thin cover also extends to the base of these slopes, suggesting that these may be active fault scarps and that sediment slumping is minimal. Corrections for the effects of topography (e.g. Lachenbruch 1968), although small, would generally tend to accentuate the observed modulation. Similarly, thermal refraction caused by the conductivity contrast between rock and sediment is small because of the uniform sediment cover. These corrections were derived for regions in which thermal conduction is dominant and it would be inappropriate to apply them if thermal convection might be important. Therefore, no attempt has been made to modify our heat-flow values for these effects. We have seen no evidence in the bottom sediment gradients for significant temporal changes in bottom water temperature. Small variations in the temperature of the bottom water with periods shorter than a few days or longer than a few years might be difficult to detect but would not significantly affect our discussion.

The pattern of heat-flow variations, and the lack of evidence for other causes, seems to require hydrothermal circulation of sea water in the crustal rocks. Lacking any high sediment temperatures that could mark a hydrothermal vent, we conclude that the areas of low heat flow represent either (1) regions where the sea water is entering the crustal rocks, if the upper boundary of the system is still open, or (2) areas above the downgoing limb of a closed convective system.

(c) *Magnitude of hydrothermal cooling.* Using the same theoretical heat-flow model illustrated in Fig. 5 (Sclater & Francheteau 1970, equation (23)), lithospheric creation

Downloaded from https://academic.oup.com/gji/article/38/3/587/674012 by guest on 20 August 2022

along the Galapagos spreading centre results in a continuous heat loss of 1100 cal s^{-1} cm^{-1} of ridge length. Of this total more than 330 cal s^{-1} cm^{-1} is released through crust less than 35 km from the axis. This is a minimum value because it is based on a conductive cooling model, and the combination of conduction and hydrothermal convection would remove heat more efficiently. The heat loss that would result if the upper 500 m of the crust were produced by extrusive lavas would account for only about 15 cal s^{-1} cm^{-1}. In this calculation we assume the lava is solidified causing each gramme to release 100 cal of latent heat and then cooled from 1250°C to 0°C which releases an additional 300 cal of sensible heat. The average of our conductive heat-flow measurements within 35 km of the axis gives 36 cal s^{-1} cm^{-1} of ridge length. This implies that more than 80 per cent of the geothermal heat released in our survey area escapes through hydrothermal vents.

(d) *Heat flow* vs. *age*. The increase of conductive heat flow southwards from the spreading centre (Fig. 5) suggests that the free exchange of water and therefore the magnitude of the hydrothermal component of heat loss decreases as sediment accumulates. Only after the sediment blanket is sufficiently thick that it begins to form an impermeable cap, as is apparently the case near the southern end of our survey, does thermal conduction become the dominant heat transfer mode at the sediment/water interface. The permeability of these ridge sediments is not known, but they apparently remain significantly penetrable to fluid flow to thicknesses of at least 50 m.

Increasing heat flux with age has been observed on other active ridges (Talwani *et al.* 1971; Hyndman & Rankin 1972). However, on the Galapagos spreading centre the measured heat flow approaches the theoretical value at a younger age. This is probably a result of the higher sedimentation rates and smoother topography, causing the upper boundary of the hydrothermal system to be sealed more quickly.

The observed thermal gradients imply the existence of large horizontal temperature variations and furthermore, that the average temperature of near surface rocks increases with age. This is contrary to what one might normally expect from a simple model.

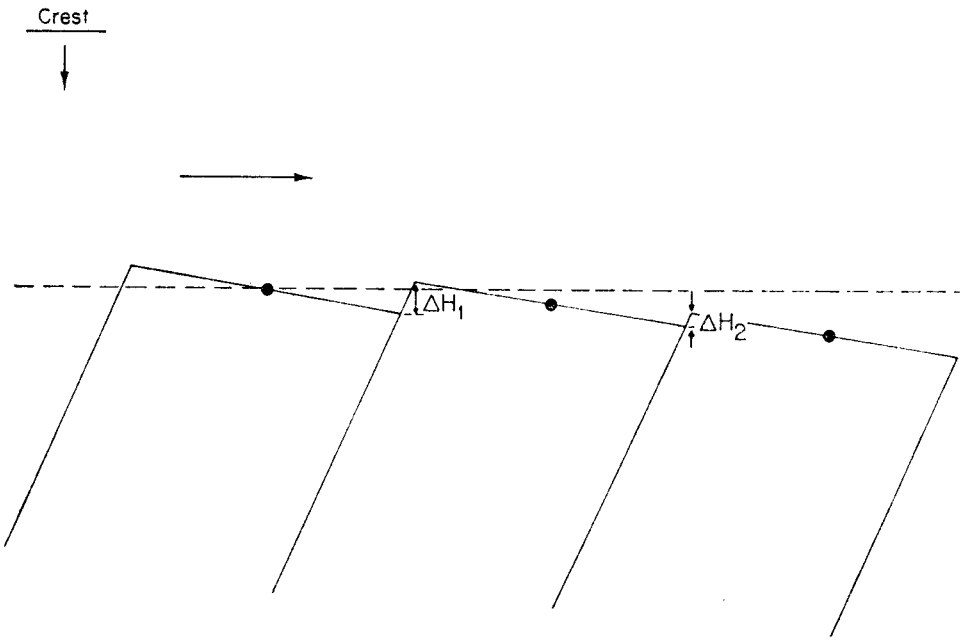

FIG. 9. Schematic representation of crestal block faulted topography. The average depth of each block increases with age whereas the scarp offset (ΔH) decreases. Dashed line indicates horizontal reference level.

Downloaded from https://academic.oup.com/gji/article/38/3/587/674012 by guest on 20 August 2022

(e) *Effect of hydrothermal circulation on crestal topography.* The crestal zone of the Galapagos spreading centre is dominated by faulted blocks tilted outward with scarps facing the crest (Fig. 9) (Klitgord and Mudie 1974). Scarps on blocks 0·25 My are offset (Δ H) an average of about 100 m, whereas those in 1·0 My old crust have a ΔH of only 50 m. Further, during this same period, the blocks increase in depth from approximately 2600–2700 m. Classical thermal contraction (Sclater & Francheteau 1970), lithospheric thickening (Williams & Poehls, in preparation) and the relaxation of dynamic uplift (Lachenbruch 1973) all predict this general decrease in elevation as the young crust ages.

Hydrothermal circulation provides us with an additional mechanism for generation of the crestal elevation changes. Circulation of sea water in the crustal blocks produces hydration of the oceanic crust. As the crustal blocks spread from the intrusion zone, portions of the blocks are reheated from below. This can produce metamorphic upgrading of the hydrous assemblage which may account for an additional overall elevation decrease. In general, low grade metamorphic rocks have larger volume changes (Δ V) of reaction than higher grade metamorphic rocks. This can be demonstrated by

Table 2.

Standard temperature and pressure, molar volumes for the reaction:

Prehnite	Chlorite	Quartz
$5\ Ca_2Al_2Si_3O_{10}(OH)_2$	$+\ Mg_5Al_2Si_3O_{10}(OH)_8$	$+\ 2SiO_2 \rightleftharpoons$
Epidote (Zoisite)	Tremolite	Water
$4Ca_2Al_3Si_3O_{12}(OH)$	$+\ Ca_2Mg_5Si_8O_{22}(OH)_2$	$+\ 6H_2O$

Component	Volume (cm^3/mole)
Prehnite	142·20 §
Chlorite	213·01 ‡
Quartz	22·69 †
Epidote (Zoisite)	136·50 †
Tremolite	272·95 †
Water	18·07 †

Volume change of solids for the reaction * = −42·05

* All volumes treated as constants.
† From Robie *et al.* (1966).
‡ Calculated from unit-cell dimensions of prochlorite from Steinfink (1958, 1961, 1962).
§ Calculated from unit-cell dimensions from Preisinger, (1965).

comparing volume changes from the upgrading of prehnite + chlorite + quartz to epidote + tremolite + water. This is a typical active ridge metamorphic suite and the reaction produces a volume change of −4 per cent (Table 2), at STP. Thermal expansion and compressibility coefficients for these universals are unknown but the low pressures and temperatures involved should make the STP calculation accurate to within $\pm$10 per cent.

Thus, if the hydrated crustal blocks are 5 km thick, less than 50 per cent of the crust undergoing this reaction would produce the entire observed elevation decrease assuming that all of the volume change goes into elevation change. Similarly, the scarp offsets may be maintained to some extent by the existence of large horizontal temperature differences within blocks and between adjacent blocks. We would expect the offset to be reduced as the crust ages and these temperature differences decrease. It is clear that hydrothermal circulation and the resulting chemical alterations can have a substantial effect on crestal topography. Until we have a better understanding of the thermal, petrologic and chemical properties of the oceanic lithosphere it will be difficult to separate these effects from those of classical thermal contraction, lithospheric thickening and dynamic uplift in controlling crestal topography.

(f) *Geographic distribution and magnitude of heat flow.* The geographical distribution of our data is insufficient to determine whether the observed variations in heat

Downloaded from https://academic.oup.com/gji/article/38/3/587/674012 by guest on 20 August 2022

flow largely are two-dimensional, like the topography, or three-dimensional. Furthermore, a theoretical model with inherent uncertainties is required to estimate the magnitude of heat released by hydrothermal circulation on the spreading centre. We can only say that this circulation appears to control the near-axis conductive heat-flow pattern and that this pattern bears only a limited relationship to the actual heat flux. In regions where the hydrothermal system still has a free exchange with the bottom water, the theoretical models provide a more realistic means to estimate the heat flux than the measured values of conductive heat flow. Even where the sediment forms an impermeable upper layer, hydrothermal circulation may persist in the crustal rocks below the sediment, which clearly requires a large number of measurements spaced significantly closer than the scale of the circulation pattern to obtain a reliable value of the regional heat flux.

Downloaded from https://academic.oup.com/gji/article/38/3/587/674012 by guest on 20 August 2022

Character of the hydrothermal system

(a) *Hydrothermal vents.* Reasonably clear evidence for hydrothermal vents is presented from the bottom water temperature anomalies of Fig. 8. With expressions developed empirically by Rouse, Yih & Humphreys (1952), and discussed by Batchelor (1954) and Turner (1969), it is possible to make a rough estimate of the heat transfer by steady-state thermal plumes of this size. The rate of heat loss F represented by a two-dimensional plume is

$$F = \left[\frac{zg'}{2.6} \exp\left(41x^2/z^2\right)\right]^{3/2} \text{ cal s}^{-1} \text{ cm}^{-1}$$

and for a three-dimensional plume

$$F = \left[\frac{z^{5/3}g'}{11} \exp\left(71r^2/z^2\right)\right]^{3/2} \text{ cal s}^{-1}$$

where $g' = \alpha g\,(T-T_0)$ with g the gravitational acceleration and T the anomalous temperature observed at distance z above the bottom and at distance x or radius r from the vertical axis of the plume. The coefficient of thermal expansion α is taken for the fluid medium at ambient temperature T_0. These equations assume that the composition of the plume water is not significantly different than the bottom water, that the plume is from a point or line source, and that is not significantly affected by bottom currents.

We estimate the anomaly near 2·76 km in Fig. 8 at 1600 ± 300 cal s^{-1} for a three-dimensional plume or $13{\cdot}4 \pm 3{\cdot}6$ cal s^{-1} cm^{-1} for a two-dimensional plume. The uncertainties derive from those associated with the temperature data. We have assumed that the profile was directly above the source, so that the values of F should be considered minimal.

Exrusive lava flows can be expected to heat the water that quenches and cools them. However, in an area as small as the one covered by our water temperature profile lava flows should be very infrequent with the lava cooling quickly. Therefore, we feel that the observed temperature anomalies are more probably caused by thermal plumes rising from hydrothermal vents.

The correlation between heat-flow maxima and the occurrence of small sediment mounds (Figs 5 and 6(d), (e) and (f) suggests that these mounds are hydrothermal vents. They seem to have no expression in the basement topography and they tend to be lineated as though they were above a hydrothermal fissure in the basement rock (Klitgord & Mudie 1974). We can only speculate about the character of the flow from these vents. It could be continuous or periodic. The fact that these mounds appear only in areas of high heat flow implies the elements of the hydrothermal system remain nearly fixed with respect to the underlying crust for long periods of time. At the observed sedimentation rates, it would take more than one hundred thousand years to

bury one of these mounds after it became inactive. Interestingly, our station 62 has combined the qualities of a relatively low thermal gradient and high sediment temperatures (Fig.10) expected of a measurement near an active hydrothermal vent (Fig. 4(b)) and is located within one of these fields of sediment mounds. This explanation of the unusual temperature–depth relation seen in Fig. 10 may be more probable than excessive superpenetration of the coring apparatus.

The heat transfers we have calculated for some of the plumes, deduced from Fig. 8, represent a significant percentage of the total regional heat loss. Yet, just a few metres above the bottom, the predicted and observed temperature anomalies are less than 0·1 °C. Larger temperature anomalies would be expected closer to the vent. Also if the vented water were warmer and more dense (due to chemical differences) than the surrounding sea water, it might collect in pools such as those found in the Red Sea.

(b) *The deep hydrothermal system.* The circulation pattern could be controlled by one or more of the following physical properties of the system: (1) variation in the strength of heat sources near the base of the crust, (2) bottom topography, (3) discrete zones of

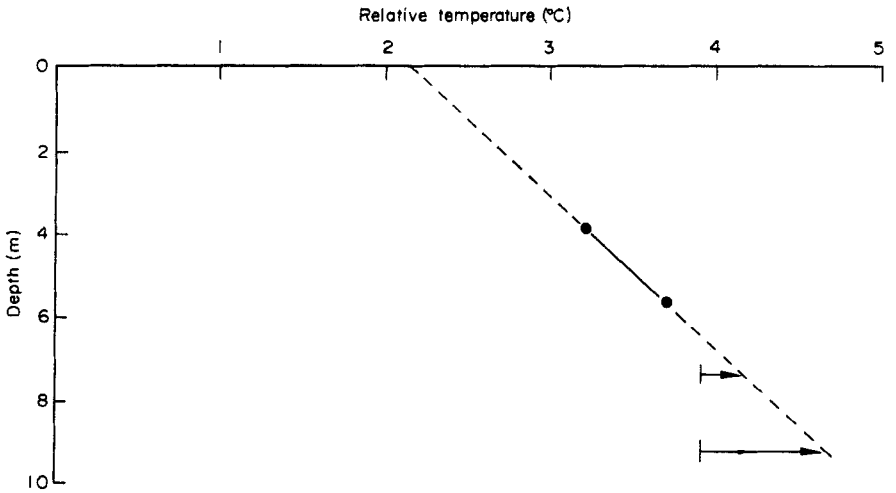

FIG. 10. Relative temperature versus depth for station 62. Depths are from the bottom of the piston corer weight stand. Any amount of superpenetration would increase these depths. Temperatures are relative to the bottom water temperature (2·04°C ± ·01°C). There were four thermistors mounted on the core barrel. The lower two, whose position are indicated by arrows, were sensing relative temperatures which were greater than 3·9°C, the highest our instrumentation was set to record.

high permeability, or (4) cellular convection. Only limited conclusions may be inferred from the heat-flow data. Hot intrusives rising to near the base of the oceanic crust, spaced at about 6 km along our track could force the entire system. The pattern of steep scarps suggests that the surface might have undergone north–south extension and block faulting which could be a by-product of deep intrusive east–west trending dikes associated with sea-floor spreading. The occurrence of heat-flow maxima near topographic highs and heat-flow minima near topographic lows may imply topographic control as proposed by Lister (1972). This correlation between topography and the heat-flow pattern, although approximate, appears to be more than a coincidence. The data seem to indicate that the convection is not entirely controlled by the major vertical faults. The heat-flow maxima and minima on the Galapagos spreading centre, are not always located near the steep scarps (faults?) (Fig. 7). This is in contrast to

Downloaded from https://academic.oup.com/gji/article/38/3/587/674012 by guest on 20 August 2022

the pipe model of Bodvarsson & Lowell (1972) and to observations in the high temperature areas of Iceland (Bodvarsson 1961) and most continental geothermal areas (McNitt 1965) where the hydrothermal activity at the surface is in close proximity to dike contacts and vertical faults (zones of high vertical permeability). This could imply that the young oceanic crustal rocks on this spreading centre, and perhaps elsewhere, have a finer scale of permeability than rocks in continental geothermal areas.

(c) *Cellular convection.* Cellular convection through permeable rock was first suggested by Elder (1965) as being the mechanism by which large amounts of heat might be removed from active ocean ridges. The apparent regularity of the modulation in heat flow has led us to consider this mechanism.

Convection in a homogeneous medium is theoretically possible whenever the critical Rayleigh number is exceeded. This dimensionless parameter R is defined by

$$R = k\,\alpha\,g\,\Delta T H/\kappa\nu$$

where the properties of the fluid saturated medium are given by permeability k, thickness h, upper to lower surface temperature difference ΔT, and thermal diffusivity κ. The properties of fluid are defined by coefficient of thermal expansion α and kinematic viscosity ν. Erickson & Simmons (1969) and Lister (1972) discuss the magnitudes of these parameters and stress that the principal unknown is the permeability. It is clear that the Rayleigh number decreases away from the ridge crest because of the inevitable decrease in the temperature differences (ΔT) and average permeability (k). Local periodic changes in the strength of the heat source will also affect the ΔT and hence the Rayleigh number. In a closed system with a plane evenly-heated lower boundary and a plane isothermal upper boundary the critical Rayleigh number is near 40 (Lapwood 1948). However, when the upper boundary is not plane, any positive Rayleigh number is above the critical value. Despite this, low Rayleigh numbers would not be expected to produce large scale flows. Elder (1965, 1967) explains how problems can be studied utilizing computer-generated solutions or laboratory modelling (e.g. Hele-Shaw cell). Other studies have been reported by Lapwood (1948), Donaldson (1962), and Wooding (1959).

Hele-Shaw (1898) showed that cellular convective motion in a horizontal slab of homogenous saturated porous material of thickness H and lateral extent L is similar to that in a vertical cavity of width $a \ll H,L$ where the permeability $k = a^2/12$. The theory may be found in Lamb (1932, section 330). Although the motion in a Hele-Shaw cell is only two-dimensional most convective motion of this type perferentially forms two-dimensional rolls and there is the great advantage that the flow can be visualized.

Utilizing a Hele-Shaw cell similar to Elder's (1965), we have attempted to model the Galapagos spreading centre problem. From the few simple experiments so far conducted, only preliminary conclusions are possible (Willams 1974). (1) It appears the ridge topography has a strong influence on the position of the cellular convection, forcing the upgoing limbs under topographic highs as seen in Fig. 11 (a). This would produce a measured heat-flow pattern similar to Fig. 6(a) and (c). The downgoing limbs are forced under topographic lows (Fig. 11(b) and (c)). (2) In the Galapagos spreading centre model, the topography seems to have very little influence over the wavelength of the cellular convection. This may be because the amplitude of the topographic undulations is much less than the depth of circulation. (3) Most studies to date (Elder 1965; Donaldson 1962; Lapwood 1948), including ours, have found that Rayleigh cells are approximately equidimensional at Rayleigh numbers near the critical value. As the Rayleigh number increases the cells gradually become less constrained to the equidimensional shape (Fig. 12). The range of stable wavelengths in a porous medium has not yet been determined. With our observed modulation wavelength of 6 km, equidimensional Rayleigh cells would penetrate approximately 3 km and greater depths are certainly possible.

Downloaded from https://academic.oup.com/gji/article/38/3/587/674012 by guest on 20 August 2022

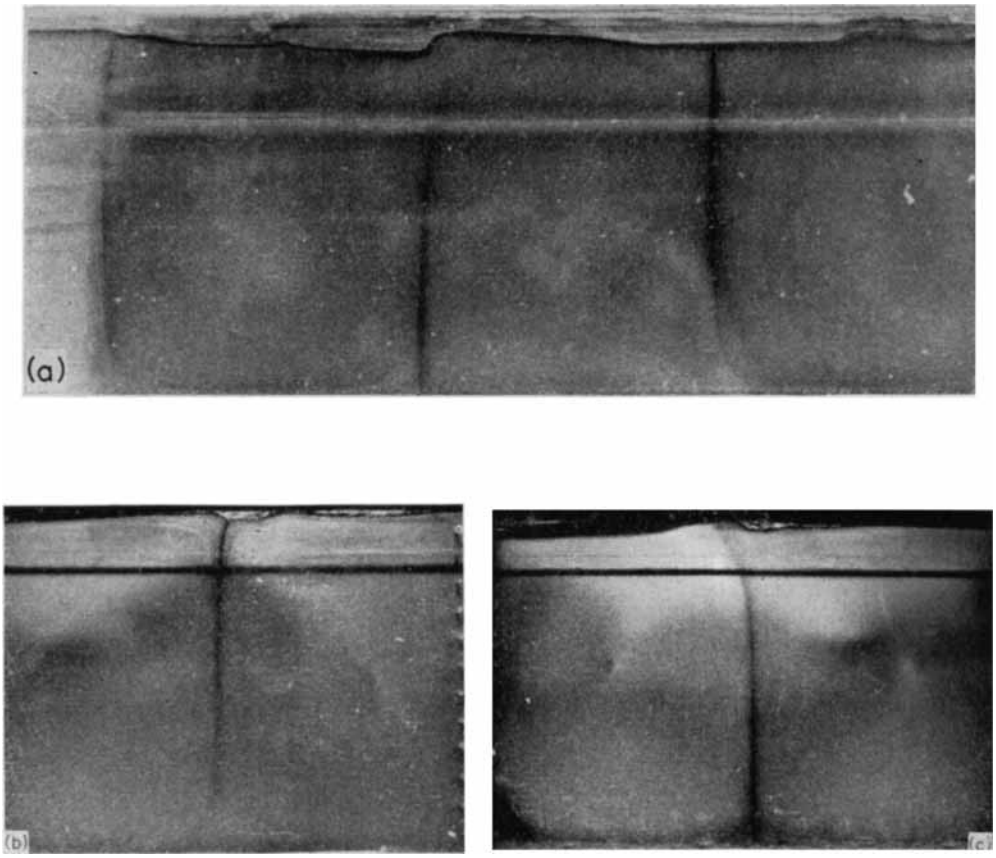

FIG. 11. Photographs illustrating the effects of topography on the motion in Hele-Shaw cell. The topography, simulating the Galapagos spreading centre, can be seen near the upper edge of the pictures and is scaled to a 3·75 km deep circulation system. The horizontal line just below this is part of the laboratory apparatus. The dark, nearly vertical lines are the rising and descending limbs of Rayleigh cells The three photographs show (a) a rising limb in the centre, flanked by two descending limbs. (b) A descending limb in a topographic low. (c) A rising limb under a topographic high. It can be seen that below the upper boundary the cells are not as rigidly constrained by the topography.

Downloaded from https://academic.oup.com/gji/article/38/3/587/674012 by guest on 20 August 2022

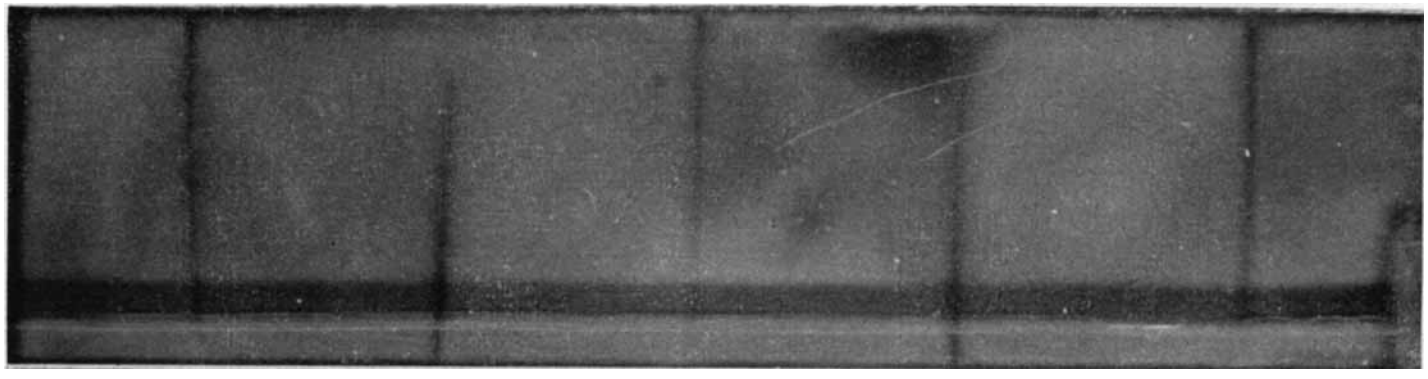

FIG. 12. Photograph of motion in a Hele-Shaw cell. There is no topography in this cell, i.e. the upper boundary is flat and closed. In this experiment the Rayleigh number was 360. From left or right the vertical dark columns are alternately rising (darkest and widest at bottom) and descending limbs.

These conclusions are primarily based on experiments with a Hele-Shaw cell modelling a completely closed and isothermal upper boundary. Preliminary experiments with a Hele-Shaw cell having an upper boundary open for free discharge and recharge have yielded similar results.

The motion in a Hele-Shaw cell is only two-dimensional. This is sufficient whenever the motion in the actual system is dominated by two-dimensional rolls. If, however, the motion were three-dimensional, the addition of another degree of freedom should tend to reduce the range of stable wavelengths but could also weaken the dependence between topography and wavelength.

This type of study, as mentioned earlier, cannot be conclusive in determining the controlling parameters of ocean ridge hydrothermal circulation. However, laboratory modelling and mathematical and numerical analysis can provide valuable insight. More work is obviously necessary in these areas before we can more accurately describe actual spreading ridge systems.

Conclusions

Lithospheric cooling along the Galapagos spreading centre at 86°W Longitude, as determined from surface heat-flow measurements, appears dominated by hydrothermal convection. The conductive heat-flow values alone do not provide an accurate estimate of the total heat flux, but if theoretical cooling models are accepted, hydrothermal convection accounts for approximately 80 per cent of the geothermal heat released along the Galapagos spreading centre through crust less than 1 My. As sediment accumulates, the rate of discharge from the hydrothermal system apparently decreases and the average of the observed heat-flow values begin to agree, in general, with theoretical conductive cooling models. The horizontal wavelength of the convective flow on the Galapagos spreading centre is 6 $\pm$1 km; water may penetrate several kilometers into the crust. The results of this study show the difficulties in resolving systematic patterns in the heat-flow distribution on spreading ridges from heat-flow surveys. If the Galapagos spreading centre is typical of these ridges, numerous, closely-spaced measurements with precise navigation combined with a relatively uniform sediment cover, appear to be necessary ingredients for recognition of the heat-flow pattern.

Acknowledgments

We would like to acknowledge the help of F. Dixon, J. Rogers, M. Hobart and V. Pavlicek who helped with, or took, many of the measurements presented in this paper. We are also indebted to Captain Bonham and the crew of the R/V Thomas Washington. We would also like to thank K. Klitgord, R. Detrick and J. Mudie for their invaluable assistance in gathering, reducing and interpreting the wealth of geophysical data gathered on legs 6 and 7 of 'South Tow'. Further, their critical review led to several improvements and additions to this paper. This research was supported by the National Science Foundation Grant GA-16078.

D. L. Williams and R. P. Von Herzen:
Woods Hole Oceanographic Institution
Woods Hole, Massachusetts 02543

R. N. Anderson:
University of California, San Diego
Marine Physical Laboratory of the
Scripps Institution of Oceanography,
La Jolla, California 92037

J. G. Sclater:
Earth and Planetary Sciences,
Massachusetts Institute of Technology
Cambridge, Massachusetts 02139

Downloaded from https://academic.oup.com/gji/article/38/3/587/674012 by guest on 20 August 2022

References

Anderson, R. N., 1972 Low heat flow on flanks of slow spreading mid-ocean ridges, *Geol. Soc. Am. Bull.*, **83,** 1947.

Aumento, F., Loncarevic, B. D. & Ross, D. I., 1971, Hudson geotraverse: geology of the Mid-Atlantic Ridge at 45°N, *Phil. Trans. Soc. Lond. A.*, **268,** 623.

Batchelor, G. K., 1954. Heat convection and buoyancy effects in fluids, *Meteoral. Soc.*, **80,** 339.

Bodvarsson, G., 1961. Physical characteristics of natural heat resources in Iceland, *Jökull*, **7,** 29.

Bodvarsson, G. & Lowell, R. P., 1972. Ocean-floor heat flow and the circulation of interstitial waters, *J. geophys. Res.*, **77,** 4472.

Boegeman, D. E. Miller, G. S., 1972. Precise positioning for near bottom equipment using a relay transponder, *Mar. geophys. Res.*, **7,** 381.

Corliss, J. B., 1971 The origin of metal-bearing submarine hydrothermal solutions, *J. geophys. Res.*, **76,** 8128.

Corry, C., Dubois C. & Vacquier, V., 1968. Instrument for measuring terrestrial heat flow through the ocean floor, *J. mar. Res.*, **26,** 165.

Deffeyes, K. S., 1970. The axial valley: a steady state feature of the terrain, in *Megatectonics of continents and oceans*, New Brunswick, Rutgers University Press.

Detrick, R. S., Williams, D. L. Mudie, J. D. & Sclater, J. G., 1974. The Galapagos Spreading Centre: bottom-water temperatures and the significance of geothermal heating *Geophys,. J.R. astr. Soc.*, **38,** 627–636.

Donaldson, I. G., 1962. Temperature gradients in the upper layers of the Earth's crust due to convective water flows, *J. geophys. Res.*, **67,** 3449.

Elder, J. W., 1965. Physical processes in geothermal areas, *Am. geophys. Un. Mono.*, **8,** 211.

Elder, J. W., 1967. Steady free convection in a porous medium heated from below, *J. fluid Mech.*, **27,** 29.

Erickson, A. J. & Simmons, G., 1969. Thermal measurements in the Red Sea hot brine pools, in *Hot brines and recent heavy metal deposits in the Red Sea*, eds E. T. Degens and D. A. Ross, Springer-Verlag, New York.

Grim, P. J., 1970. Connection of Panama fracture zone with the Galapagos rift zone, eastern tropical Pacific, *Mar. geophys. Res.*, **1,** 85.

Hele-Shaw, H. S. J., 1898. *Trans. Inst. Naval Architects*, **40,** 21.

Herron, E. M., 1972. Sea-floor spreading and the Cenozoic history of the east–central Pacific, *Geol. Soc. Am. Bull.*, **83,** 1671.

Herron, E. M. & Heirtzler, J. R., 1967, Sea-floor spreading near the Galapagos, *Science*, **158,** 775.

Hey, R. N., Deffreyes, K. S., Johnson, G. L. & Lowrie, A., 1972. The Galapagos triple junction and plate motions in the east Pacific, *Nature*, **237,** 20.

Hyndman, R. D. & Rankin, D. S., 1972. The Mid-Atlantic Ridge near 45°N XVIII: Heat-flow measurements, *Can. J. earth Sci.*, **9,** 664.

Klitgord, K. D. & Mudie, J. D., 1974. The Galapagos Spreading Centre: a near-bottom geophysical study, *Geophys. J. R. astr. Soc.* **38,** 563–586.

Lachenbruch, A. H., 1968. Rapid estimation of the topograhic disturbance to superficial thermal gradients, *Rev. Geophys.*, **6,** 365.

Lachenbruch, A. H., 1973. A simple mechanical model for oceanic spreading centers *J. geophys. Res.*, **78,** 3395.

Lamb, H., 1932. *Hydrodynamics*, Cambridge University Press, London.

Langseth, M. G., LePichon, X. & Ewing, M., 1966. Crustal structure of mid-ocean ridges. 5. Heat flow through the Atlantic Ocean floor and convection currents, *J. geophys. Res.*, **71,** 5321.

Downloaded from https://academic.oup.com/gji/article/38/3/587/674012 by guest on 20 August 2022

Langseth, M. G. & Von Herzen, R. P., 1971. Heat flow through the floor of the world oceans, in *The Sea*, Volume 4, Part 1, ed. A. E. Maxwell, Wiley-Interscience, 299.

Lapwood, E. R., 1948, Convection of a fluid in a porous medium, *Proc. Camb. phil. Soc.*, **44,** 508.

Lee, W. H. K., 1970, On the global variations of terrestrial heat flow, *Phys. Earth Planet. Int.*, **2,** 332.

Le Pichon, X. & Langseth, M. G., 1969. Heat flow from mid-ocean ridges and sea-floor spreading, *Tectonophys.*, **8,** 319.

Lister, C. R. B., 1972. On the thermal balance of a mid-ocean ridge, *Geophys. J. R. astr. Soc.*, **26,** 515.

McKenzie, D. P., 1967. Some remarks on heat flow and gravity anomalies, *J. geophys. Res.*, **72,** 6261.

McKenzie, D. P. & Sclater, J. G., 1969. Heat flow in the eastern Pacific and sea-floor spreading, *Bull. Volcanologique*, **33–1,** 101.

McNitt, J. R., 1965. Review of geothermal resources, *Am. geophys. Un. Mono.*, **9,** 240.

Nishimori, R. K. & Anderson, R. N., 1974. Gabbro, serpentinite, and mafic breccia from the East Pacific, *Earth planet. Sci. Lett.* in press.

Miyashiro, A., Shido, F. & Ewing, M., 1971. Metamorphism in the Mid-Atlantic Ridge near 24° and 30°N, *Phil. Trans. R. Soc. Lond. A.*, **268,** 589.

Pálmason, G., 1967. On heat flow in Iceland in relation to the Mid-Atlantic Ridge, *Visindafjelay Islendinaga*, Ret. 1967 Rep. of a symposium, Geoscience Soc., Iceland, Reykjavik, 111.

Parker, R. L. & Oldenburg, D. W., 1973. Thermal model of ocean ridges, *Nature*, **242,** 137

Preisinger, A., 1965. Prehnite—ein Schichtsilikatty, *Tschermaks Mineral Petrg. Mitt.*, **10,** 491–504.

Raff, A. D., 1968. Sea-floor spreading: Another rift, *J. geophys. Res.*, **73,** 3699.

Robie, R. A., Bethke, P. M., Toulmin, M. S. & Edwards, J. L., 1966, X-ray crystallographic data, densities, and molar volumes of minerals: *Geol. Soc. Am. Bull., Mem.* **97,** 27–73.

Rouse, H., Yih, C-S & Humphreys, H. W., 1952, Gravitational convection from a boundary source, *Tellus*, **4,** 201.

Sayles, F. L. & Bischoff, J. L., 1973, Ferromaganoan sediments in the equatorial East Pacific, *Earth Planet. Sci. Lett.*, **19,** 330.

Sclater, J. G. & Francheteau, J., 1970. The implications of terrestrial heat flow observations on current tectonic and geochemical models of the crust and upper mantle of the Earth, *Geophys. J. R. astr. Soc.*, **20,** 509.

Sclater, J. G. & Klitgord, K. D., 1973. A detailed heat flow, topographic and magnetic survey across the Galapagos spreading centre at 86°W, *J. geophys. Res.*, **78,** 6951.

Sleep, N. H., 1969. Sensitivity of heat flow and gravity to the mechanism of sea-floor spreading, *J. geophys. Res.*, **72,** 542.

Spooner, E. T. C. & Fyfe, W. S., 1973. Sub-sea-floor metamorphism, heat and mass transfer, *Contr. Mineral. Petrol.* **42,** 287.

Steinfink, H.,1958. The crystal structure of Chlorite. II. A triclinic polymorph: *Acta Cryst.*, **11,** 195–198.

Steinfink, H., 1961. Accuracy in structure analysis of layer silicates: Some further comments on the structure of prochlorite: *Acta Cryst.*, **14,** 198–199.

Steinfink, H., 1962 A correction—the crystal structure of Chlorite. I. A monoclinic polymorph: *Acta Cryst*, **15,** 1310.

Talwani, M., Windisch, C. C. & Langseth, M. G., 1971. Reykjanes ridge crest: a detailed geophysical study, *J. geophys. Res.*, **76,** 473.

Turner, J. S., 1969. Buoyant plumes and thermals, *Ann. Rev. fluid Mech.*, **1.** 29.

Downloaded from https://academic.oup.com/gji/article/38/3/587/674012 by guest on 20 August 2022

van Andel, T. H. & Heath, G. R., 1973. *Initial reports of the Deep Sea Drilling Project*, Vol. 16, Washington, D. C. (U.S. Government Printing Office).

van Andel, T. H., Heath, G. R., Malfait, B. T., Heinrichs, D. F. & Ewing, J. L., 1971, Tectonics of the Panama basin eastern equatorial Pacific, *Geol. Soc. Am. Bull.*, **82,** 1489.

Von Herzen, R. P. & Maxwell, A. E., 1959. The measurement of thermal conductivity of deep sea sediments by a needle-probe method. *J. geophys. Res.*, **64,** 1557.

Von Herzen, R. P. & Anderson, R. N., 1972, Implications of heat flow and bottom water temperature in the eastern equatorial Pacific, *Geophys. J. R. astr. Soc.*, **26,** 427.

Von Herzen, R. P. & Langseth, M. G., 1966, Present status of oceanic heat flow measurements, *Phys. Chem. Earth*, **6,** 365.

Von Herzen, R. P. & Uyeda, S., 1963, Heat flow through the eastern Pacific Ocean floor, *J. geophys. Res.*, **67,** 4219.

Williams, D. L. & Von Herzen, R. P., 1974. Heat loss from the Earth; New estimate, *Geology*, **2,** 327.

Williams, D. L., 1974. *Heat loss and hydrothermal circulation due to sea-floor spreading*, Ph.D. Thesis, Woods Hole Oceanographic Institution, Woods Hole, Massachusetts, 139p.

Wooding, R. A., 1960. Instability of a viscous liquid of variable density in a vertical Hele-Shaw cell, *J. fluid Mech.*, **7,** 501.

Downloaded from https://academic.oup.com/gji/article/38/3/587/674012 by guest on 20 August 2022